MM-Wave Radar Vitals Sensing: Towards Non-Contact Cardiac and Respiratory Gating for MRI

Hemal Arora[1], Fraser Robb[2], Shreyas Vasanawala[3], John Pauly[1], and Greig Scott[4]
[1]Stanford University, Stanford, CA, United States, [2]GE Healthcare, Aurora, OH, United States, [3]Radiology, Stanford University, Stanford, CA, United States, [4]Electrical Engineering, Stanford University, Stanford, CA, United States

Synopsis

Motivation: Present day cardiac and respiratory gating require cabled sensors that impede patient workflow. A non-contact sensing method is needed.

Goal(s): Our goal is to determine whether non-contact mm-wave radar neck vessel motion sensing can distinguish the cardiac cycle from respiratory motion with a long term aim of non-contact gating.

Approach: We updated a 4 channel 24GHz CW radar system using dual Analog Discovery Pros for chest/neck data capture and integrated ECG monitoring with Python scripting.

Results: Respiratory motion remains easily detected with high SNR. Neck vessel motion creates unique waveforms with carotid notch and jugular venous pulse contributions variably mixed.

Impact: MM-wave radar is a promising candidate for non-contact sensing of cardiac and respiratory cycles, with potential applications in non-contact motion gating in pediatric MRI and synchronizing on pulsatile motion of the cerebrum in neuroimaging.

Introduction

Magnetic Resonance Imaging (MRI) relies on Electrocardiograms (ECGs) and respiratory bellows to synchronize image acquisition with the patient's cardiac and respiratory cycles, thereby reducing motion artifacts in reconstructed images. However, within the MRI environment, ECG signals are susceptible to distortion from the Magnetohydrodynamic (MHD) effect and by interference from gradients [1]. Additionally, ECG leads, which make direct contact with the patient's skin, can absorb radio frequency pulses, which poses a risk of RF burn injuries [2,3]. Such direct-contact vital signs sensing methods also increase setup times and contribute to patient discomfort during scans. Pilot tone methods [4-6] address these issues but cannot operate independently of the MRI receive chain, while radars can [7-9]. We propose a non-contact approach for monitoring respiratory and cardiac cycles using an array of four 24 GHz continuous wave radars positioned above the patient's neck and chest, building on prior work in this area [10-12]. This system is highly sensitive to small motions, enabling the detection of subtle vibrations associated with the Carotid Artery and Jugular Venous Pulse (JVP) at the neck, as well as atrial and ventricular vibrations and bulk respiratory motion at the chest. Across 80 tests with two volunteers, we evaluated the robustness of these signals as a potential alternative for reliable vital signs capture for future deployment in MRI.

Hardware Methods

Our radar test bench uses RFBeam K-LC5 24 GHz mm-wave radar transceivers mounted on adjustable arms and positioned approximately 5 cm above the left and right sides of the neck and chest. To amplify the raw radar signals, we designed and fabricated custom printed circuit boards (PCBs) incorporating a 10x DC gain stage, which interfaced with a pair of Digilent Analog Discovery Pro digitizers for analog-to-digital conversion. For ground truth cardiac measurements, we employed Sparkfun ECG and PulseSensor PPG sensors connected to a Digilent Analog Discovery 2 digitizer. All sensors were synchronized using a unified trigger.

Radar Signal Processing

Radar, ECG, and PPG data were sampled at 10 kHz over a 10-second period for each experiment. To reduce computational overhead, we decimated the data by a factor of 100. Singular Spectrum Analysis (SSA) was then applied to the radar IQ data with a window length set to one-fourth of the data length. To isolate heartbeat waveforms, we generally excluded the first Reconstructed Component (RC), which typically represented bulk motion, and reconstructed the signal with RCs 2-20, effectively creating a data-driven filter. After SSA, the complex IQ data was rotated along its principal components and fit to a circular arc. Finally, Independent Component Analysis (ICA) was applied for unsupervised separation of respiratory and cardiac waveforms.

Results

During breath-hold tests, we consistently captured the carotid pulse and jugular venous pulse (with distinct a, c, and v waves along with x and y descents), solely using SSA reconstruction with RCs 2-20. These results demonstrate that high-fidelity pulsatile signals are achievable from neck radars, despite the low-pressure nature of the JVP. Additionally, SSA successfully captured cardiac vibrations in the chest, providing a view into atrial and ventricular systole and diastole. ICA further separated more complex differential and common-mode motions between the left and right radar pairs at both the neck and chest.

In free-breathing tests, neck signals continued to capture carotid and jugular pulsations after SSA reconstruction while chest signals predominantly captured respiratory motion, enabling clear tracking of breathing. Recognizing that respiratory motion dominated the first three RCs of the chest signals, we selectively reconstructed them with RCs 4-20 and applied ICA to isolate cardiac signals from the chest, resulting in components that aligned well with the ECG and PPG signals.

Discussion

Our findings demonstrate that mm-wave radar can effectively capture high-fidelity carotid pulse and JVP signals, even under free-breathing. These waveforms reflect the left ventricle output and right atrium input, and could be valuable for synchronizing neuroimaging with cardiac pulses. We also captured cardiac signals from the chest during breath-hold tests, though they were generally obscured by respiratory motion during free breathing. Selective reconstruction in SSA enabled cardiac signal extraction from the chest under free breathing, though reproducibility with this method remains a challenge.

Conclusion

This study highlights the potential of mm-wave radar as a non-contact method for cardiac and respiratory gating. Further work is motivated to investigate the signals extracted via ICA, enhance the robustness of cardiac signals from the chest during free breathing, and explore the potential for synchronizing neuroimaging with neck vessel signals, with integration into deep learning-based image reconstruction algorithms.

Acknowledgements

The authors would like to thank GE Healthcare for research support, and acknowledge funding from NIH grants R01EB019241, U01EB029427, R01EB012031, U01EB026412, R01EB009690, R01EB035109.

References

[1] J. W. Krug and G. Rose, "Magnetohydrodynamic distortions of the ECG in different MR scanner configurations," 2011 Computing in Cardiology, Hangzhou, China, 2011, pp. 769-772.

[2] S Abdel-Rehim, S Bagirathan, S Al-Benna, C O'Boyle. Burns from ECG leads in an MRI scanner: Case series and discussion of mechanisms. Ann Burns Fire Disasters. 2014;27(4):215-218.

[3] M Tang, T Yamamoto. Progress in Understanding Radiofrequency Heating and Burn Injuries for Safer MR Imaging. Magn Reson Med Sci. 2023;22(1):7-25. doi:10.2463/mrms.rev.2021-0047

[4] T Vahle, M Bacher, D Rigie, M Fenchel, P Speier, J Bollenbeck, KP Schafers, B Kiefer, and FE Boada. Respiratory Motion Detection and Correction for MR Using the Pilot Tone. Invest. Radiol., 55:153–159, 2020.

[5] J Ludwig, P Speier, F Seifert, T Schae!ter, and C Kolbitsch. Pilot Tone-Based Motion Correction of Prospective Respiratory Compensated Cardiac Cine MRI. Magn. Reson. Med., 85:2403–2416, 2021. doi:10.1002/mrm.28580.

[6] S Anand, M Lustig. Beat Pilot Tone: Exploiting Preamplifier Intermodulation of UHF/SHF RF for Improved Motion Sensitivity over Pilot Tone Navigators, ISMRM 2021.

[7] K Okamoto, T Ohishi, S Kato, R Nanaumi, K Oyama, K Fukutani, Triggering pulse generation by non-contact monitoring of heart rate using an antenna with 600 MHz resonance, p4272 ISMRM 2021

[8] E Thiel O Kosch F Seifert, Ultra-Wideband Sensors for Improved Magnetic Resonance Imaging, Cardiovascular Monitoring and Tumor Diagnostics, Sensors 10, 10778-10802, 2010.

[9] W Lee, K Ryu, Z Li, J Oscanoa, Y Wu, F Robb, S Vasanawala, J Pauly, G Scott, MRI retrospective respiratory gating and cardiac sensing by CW Doppler radar: a feasibility study, IEEE Trans Biomed Eng, accepted July 2024.

[10] T. B. Conroy, J. Zhou and E. C. Kan, "Jugular Venous Pulse Waveform Extraction From a Wearable Radio Frequency Sensor," in IEEE Sensors Journal, vol. 23, no. 9, pp. 10140-10148, 1 May, 2023, doi: 10.1109/JSEN.2023.3261548.

[11] S Suzuki , M Hoshiga, K Kotani, and T Asao, (2021) Assessment of Non-Contact Measurement Using a Microwave Sensor to Jugular Venous Pulse Monitoring. Journal of Biomedical Science and Engineering, 14, 94-102. doi: 10.4236/jbise.2021.143010.

[12] L Hughes, F Robb, S Vasanawala, J Pauly, G Scott, Four-Channel MM-Wave Radar Testbed for Neck vs Chest Cardiac Sensing, Proc 31st ISMRM, p677 Singapore 2024.

Figures

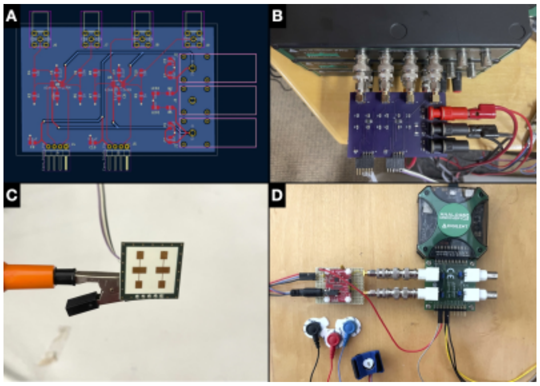

Figure 1: (A) Layout of the custom radar interface PCB, featuring a 10x gain stage for signal amplification. (B) Fabricated PCB connected to Digilent Analog Discovery Pro Digitizers. (C) K-LC5 24 GHz Radar Module. (D) Ground truth cardiac data collection setup with ECG leads and a PPG sensor, connected to a Digilent Analog Discovery 2 Digitizer.

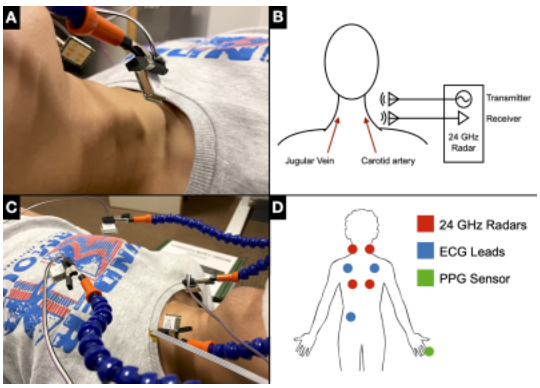

Figure 2: (A) Close-up view of 24 GHz radar placement on the neck, positioned over the jugular vein and carotid artery. (B) Schematic of the radar sensing method, highlighting vascular targets in the neck. (C) Broader view of radar transceivers positioned ~5 cm above the neck and chest. (D) Placement diagram of the positions of the 24 GHz radars (red), ECG leads (blue), and fingertip PPG sensor (green) used for synchronized data collection.

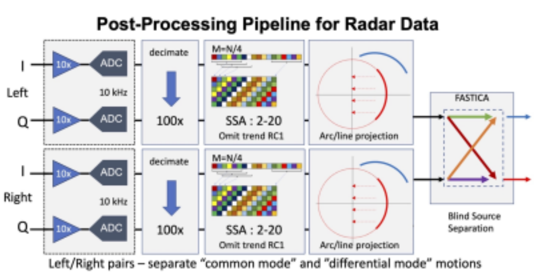

Figure 3: Post-processing pipeline for radar data. Left/Right radar channel pairs from the neck and chest are amplified, digitized at 10 kHz, and decimated 100x. Singular Spectrum Analysis (SSA) is applied and signals are reconstructed with RCs 2-20, excluding the trend (RC1). An arc/line projection then extracts motion patterns, followed by Fast Independent Component Analysis (FASTICA) for unsupervised signal source separation.

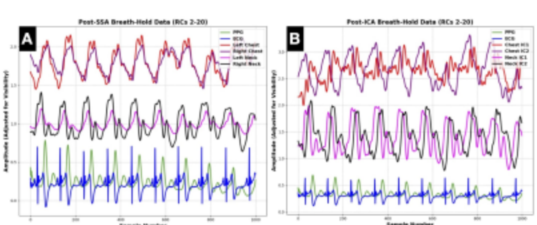

Figure 4: Comparison of SSA and ICA data during a 10 second breath-hold. (A) SSA data (including RCs 2-20) effectively extracts jugular vein and

carotid artery pulsations from left and right neck signals, as well as chest vibrations aligned with ECG/PPG signals. (B) Post-ICA data further extracts common and differential mode vibrations that align well with the frequency of the ECG/PPG signals.

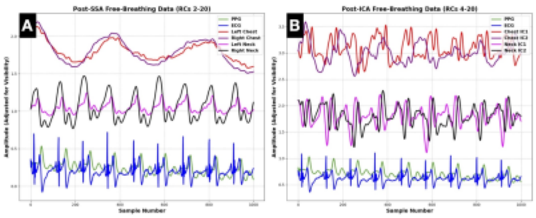

Figure 5: Comparison of SSA and ICA data during 10 seconds of free-breathing. (A) SSA data (including RCs 2-20) captures high-quality cardiac signals from the jugular vein and carotid artery, though chest motion is dominated by respiratory motion, limiting cardiac visibility. (B) Post-ICA data (RCs 4-20), with RCs 1-3 excluded due to respiratory dominance, reveals cardiac vibrations synchronized with ECG/PPG signals from the chest, while the neck channels continue to capture cardiac signals.